Modeling the mechanical properties of DNA nanostructures

Jean Michel Arbona,* Jean-Pierre Aimé, and Juan Elezgaray
CBMN, UMR 5248, CNRS, 2 rue Robert Escarpit, 33600 Pessac, France
(Received 31 August 2012; published 21 November 2012)

We discuss generalizations of a previously published coarse-grained description [Mergell *et al.*, Phys. Rev. E **68**, 021911 (2003)] of double stranded DNA (dsDNA). The model is defined at the base-pair level and includes the electrostatic repulsion between neighbor helices. We show that the model reproduces mechanical and elastic properties of several DNA nanostructures (DNA origamis). We also show that electrostatic interactions are necessary to reproduce atomic force microscopy measurements on planar DNA origamis.

DOI: 10.1103/PhysRevE.86.051912 PACS number(s): 87.15.Cc, 87.14.gk

I. INTRODUCTION

DNA nanostructures are emblematic self-organizing molecular systems exhibiting a wealth of applications, from which plain functionalized templates, computing nanomachines, and robots can be designed. Mixing different kinds of short strands may lead to rather different structures such as large ribbons [1], polyhedra [2,3] and two-dimensional lattices [4]. Using the strategy that leads to the so-called DNA origamis [5] (one very long strand folded with the help of a family of short strands), a large variety of two- and three-dimensional [6–8] constructions could also be obtained. In both cases, the robustness and high yield of the process relies on the unique selectivity of DNA base pairing.

Here, we want to modelize mechanical properties of DNA based origamis (oDNA). A detailed, atomic level description of such structures is clearly beyond the reach of current computing capabilities. Instead, we want to develop a coarse-grained description that relies on the vast corpus of experimental data acquired in the last twenty years to describe the nanomechanical properties of individual DNA molecules [9–13]. Two types of models are usually invoked to explain these single molecule experiments. Models that work at the base level [14–17] describe the energetics of stacking of neighboring base pairs as a function of geometric parameters such as twist, rise, slide, or roll. Recently, slightly more detailed models achieved significant progress in the description of dynamical processes, such as strand displacement [18].

Continuous models, such as the wormlike chain model (WLC) [19,20], work at scales larger than the helical pitch. Variations of the WLC model describe accurately not only the mechanical properties of single DNA molecules [21] but also biologically relevant phenomena such as supercoiling [22,23] or the wrapping around histone proteins [24]. Compared to these studies, the modeling of DNA based nanostructures, such as planar or 3D origamis, is still in development. First studies [25–27] focused on simple mechanical models where helices are replaced by homogeneous cylinders with the same bending rigidity as dsDNA. As DNA origamis are made of helix bundles interconnected with Holliday-like connections, additional links between the cylinders need to be introduced. References [25–27] describe how such connections can be described by continuous models. More recently, Monte Carlo simulations of wormlike chains have been shown to accurately describe the bending and torsional rigidities of helix bundles as measured by magnetic tweezers [28]. The same authors also considered finite-element-method simulations of the same helix bundle and showed almost quantitative agreement with the experimental data. Reference [29] considers a finite-element representation of DNA origamis, where each base pair corresponds to a two-node element with appropriate elastic characteristics (bending, stretching, and torsion). The authors successfully compare static and thermal fluctuations to TEM observations. It should be pointed out that none of these models of DNA origamis includes electrostatic interactions.

The purpose of the present work is to adapt an existing coarse-grained model of DNA [30] in order to model DNA origamis at the level of individual base pairs. We wish to obtain the mechanical properties (such as the persistence length of the origami) as a consequence of this modeling, and not as free parameters to be adjusted in the model. It is also expected that more accurate experimental characterizations of DNA origamis will point to the limits of continuous mechanical models such as [29]. Figure 1 illustrates this point. It shows an atomic force microscopy (AFM) image of the Rothemund's rectangular origami, deposited on mica and imaged in buffer solution. This image does not show an array of straight cylinders. Instead, helices in the assembled structures seem to bend gently to meet at crossovers as [31] suggests for similar structures. We show in the following that this deformation of the helices cannot be explained by a purely mechanical model and that electrostatic repulsion is needed.

The rest of the paper is organized as follows. In Sec. II, we describe the model and the algorithmic details. In Sec. III, we test the twist and electrostatic parameters against experimental data. In Sec. IV, we consider the measurement of the persistence length for several structures formed by bundles of DNA helices. In the last section some conclusions are drawn.

II. MODEL OF STACKED PLATES

A. Energy model

This section describes the basic ingredients of the "stack of plates" (SOP) model of dsDNA, as developed in Ref. [30]. In the SOP model, one dsDNA helix is modelled as a set of stacked objects with ellipsoidal shape; each ellipsoid represents a pair of bases. Indeed, as shown by Lavery and co-workers [32], base pairs effectively behave as rigid objects.

*jeanmichel.arbona@gmail.com

 ©2012 American Physical Society

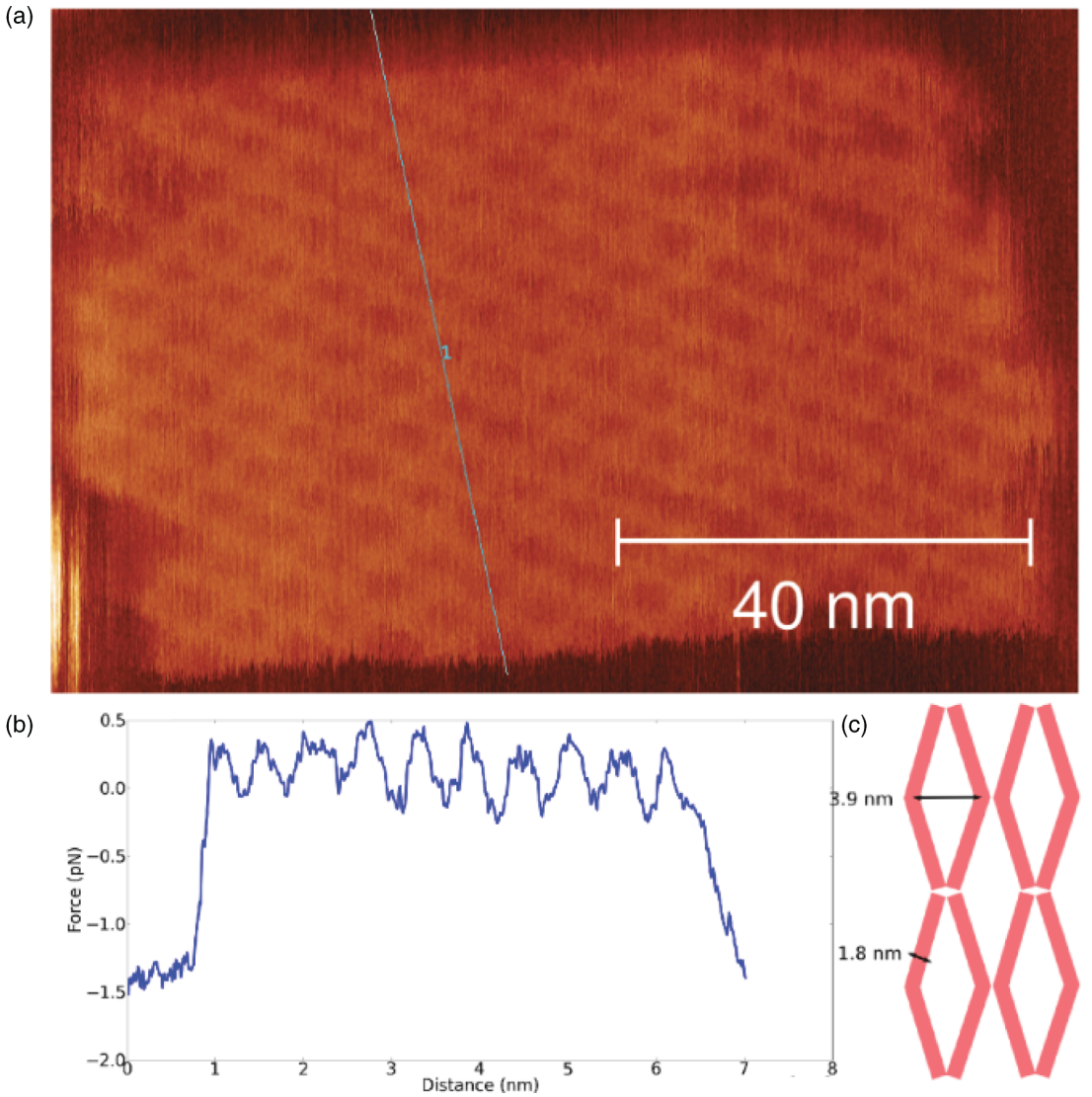

FIG. 1. (Color online) (a) AFM imaging of a rectangular origami, (b) section of the AFM picture, (c) schematic representation of the dsDNA strands as measured by AFM.

The sugar-phosphate bonds between bases are modelled as elastic springs. An illustration of the coarse-graining procedure is given in Fig. 2. The helical pattern observed in dsDNA can be understood as a compromise between the contradictory requirements of minimizing both the spring energy (equilibrium length 6 Å) and the stacking energy (minimum at 3.3 Å). The resulting average rotation between successive base pairs is close to 36°. A fine tuning of this parameter will be discussed below, as its precise value can be of importance in the modeling of DNA origamis. This model is a coarse-grained one: there is no difference between small and large grooves. Also, the model does not differentiate between left and right handed helices (this requires left handed configurations to be rejected in the sampling; see below). The reader is directed to Ref. [30] for the precise form of the interactions between plates and the values of the different parameters of the model. As discussed in Ref. [30], the SOP model is quite accurate in describing the mechanical properties of dsDNA—in particular the force-elongation characteristics.

The original SOP model does not include interactions between different strands. To take them into account, we add an interaction of excluded volume between strands: any configuration with negative distance between ellipses that belongs to different DNA strands is rejected. The function used to evaluate the distance between ellipses is an approximation of the exact expression [30]. However, this excluded volume interaction is not enough to reproduce the AFM measurements illustrated in Fig. 1.

Because each phosphate group bears a negative charge, electrostatic interactions between neighbor helices need to be taken into account (the intrastrand electrostatic interaction is effectively included in the spring contribution). The electrostatic interaction between dsDNA molecules has been the subject of an important number of experimental and theoretical work. A summary and extensive bibliography can be found in Ref. [33]. These interactions bring into play counterions. Depending on their charge and size, interactions between DNA helices can range from repulsive (single charged

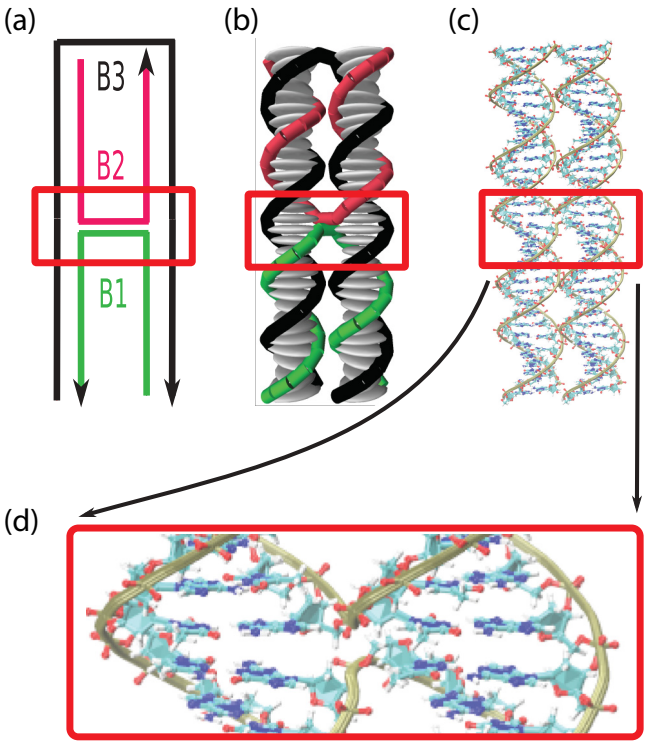

FIG. 2. (Color online) Representation of the different levels of description for a small origami, made of three single strands of DNA, noted respectively B_1, B_2, and B_3. (a) Scheme showing the connectivity of the ensemble: both B_1 and B_2 bind to B_3 (the scaffold), B_1 binds to two noncontiguous subsets of B_3. (b) SOP representation of this construction. Ellipses (in gray) representing base pairs are connected by springs (corresponding to the sugar-phosphate backbone, represented by cylinders). (c) Atomistic (ball and stick) representation. A ribbon has been superimposed to the sugar-phosphate backbone. (d) Zoom of the crossover region.

ions) to attractive (DNA condensation in the presence of multivalent ions). The situation is particularly confusing for magnesium, the counterion usually present in DNA origami experiments. For instance, molecular dynamics simulations [34] and small-angle x-ray scattering experiments [35] show that short DNA fragments (tens of base pairs) attract in a $MgCl_2$ electrolyte. Under different experimental conditions but always with Mg, other experiments do not show DNA condensation. Molecular dynamics simulations [34] show that parallel neighbor helices orient in such a way that a Mg ion bridges two opposing phosphates, resulting in an attractive interaction. Such situations are not likely to happen in DNA origamis. Contrarily to the usual experiments where DNA double helices are free to rotate one with respect to the other, in DNA origamis the crossovers determine the relative orientation of neighbor helices. Therefore, in the following we will adopt a simple modeling of electrostatics, placing a negative charge at each phosphate location (two extremities of the ellipsoid) and assuming that the effect of counterions is taken into account by a Debye type screening. This model rules out any counterion correlation contribution and leads to the repulsive interaction

$$E_{SC}(r) = e^{-r/\lambda_D(T)} \frac{q^2}{4\pi\epsilon_0\epsilon_r(T)r}, \tag{1}$$

where

$$\lambda_D(T) = \left(\frac{\epsilon_0\epsilon_r(T)k_BT}{c_0q_c^2} \right)^{1/2}$$

is the Debye length at temperature T in the presence of a concentration c_0 of counterions with charge q_c in a medium characterized by a dielectric constant $\epsilon_0\epsilon_r(T)$. k_B denotes the Boltzmann constant.

B. Monte-Carlo sampling

Once an energy model has been defined, the sampling method of the space configuration needs to be defined. We used Monte Carlo sampling [36] with the usual Metropolis criterion to sample the configuration space defined by the

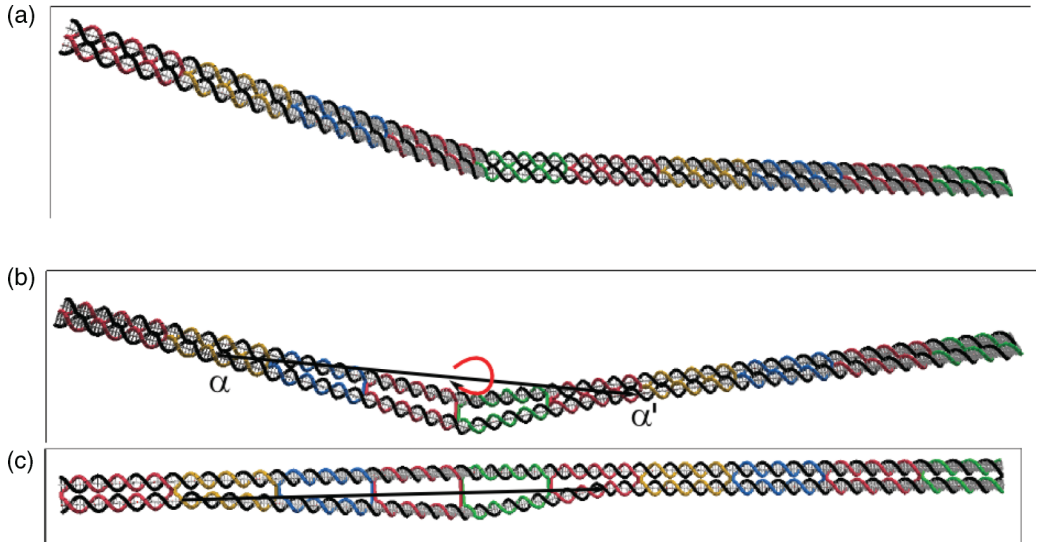

FIG. 3. (Color online) Illustration of the global Monte Carlo moves used in this paper. The structure before the move is made of two parallel straight helices linked by nine crossovers. (a) The structure after a pivot move. Panels (b) and (c) illustrate the structure after application of a crankshaft move to the structure in (a). For this move, two randomly selected bases (noted α and α') define an axis of rotation. (b) Side view, (c) top view.

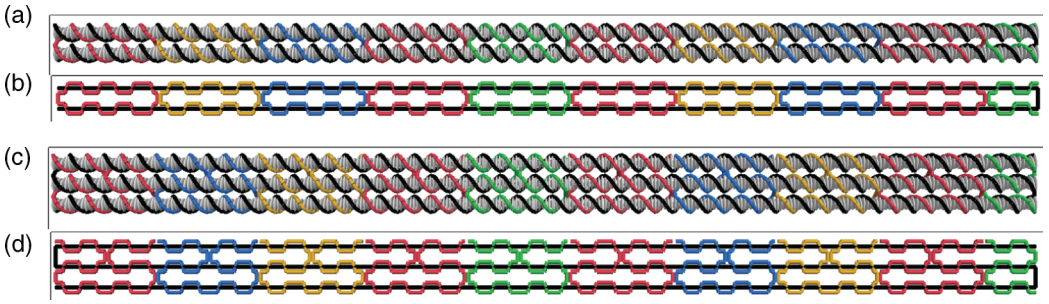

FIG. 4. (Color online) Structure of the (a) 2-oDNA(298) and (c) 3-oDNA(298) structures. Panels (b) and (d) are alternative schematic representations of respectively the 2-oDNA(298) and 3-oDNA(298) structures that highlight the topology of the crossovers. Each color corresponds to a different staple.

SOP model. Besides the local moves (translation and rotation of individual ellipsoids), we also considered "global" moves, namely pivot and crank-shaft moves. In the SOP model, the orientation of each base pair (ellipsoid) α is characterized by three unit vectors $(\mathbf{t}(\alpha),\mathbf{b}(\alpha),\mathbf{n}(\alpha))$, $\mathbf{t}(\alpha)$ being the normal vector to the plane containing each base pair. Let us denote $\mathbf{r}(\alpha)$ as the center of mass of base pair α. In a pivot move, a base pair α is chosen randomly, as well as an angle and axis of rotation, the latter being in the plane spanned by $\mathbf{b}(\alpha)$ and $\mathbf{n}(\alpha)$. The base pairs of the structure are then either located on one or the other side of this plane [considered to be centered at $\mathbf{r}(\alpha)$]. The same rotation is then applied to all the bases located on one side of this plane. An example of such a move is illustrated in Fig. 3(a).

In a crank-shaft move [Figs. 3(b) and 3(c)], two bases α and α' are chosen randomly. A rotation of random amplitude around the axis defined by $(\mathbf{r}(\alpha),\mathbf{r}(\alpha'))$ is applied to all the base pairs located between α and α'. The parameters of the Monte Carlo sampling (for instance, the maximum amplitude of the translations or the rotations) are chosen so that an average 40% acceptance ratio is obtained.

C. Umbrella sampling

In order to check the reliability of the model, we also considered equilibrium simulations under constraint. These are intended to mimic experimental situations (magnetic tweezers) where characteristics such as the distance between the opposite sides of the oDNA are constrained to a fixed value. To this end, we used umbrella sampling simulations [37,38].

The umbrella sampling allows the exploration of a restrained part of the phase space by rejecting moves that lead to configurations outside this region. This amounts to adding an "umbrella potential" that biases the Monte Carlo trajectory to sample only the configurations of interest. In this paper, we will consider the behavior of origami structures as a function of their end to end distance (R_{ee}). A standard Metropolis algorithm would typically explore configurations with an end to end distance $R_{ee} \sim R_{ee}^{eq}$ close to the equilibrium value. To explore the structure behavior for other values of R_{ee}, let us say $R_{ee} \in [l,l+dl]$, the umbrella sampling (i) generates initial configurations in this interval and (ii) runs the usual Metropolis algorithm rejecting configurations outside the interval. We obtain in this way the probability distribution of having a given end to end distance R_{ee} in a specific interval [37]. The free energy can be computed as $\beta A\,(R_{ee} \in [l;l+dl]) = -\ln[p(R_{ee})] + cst(l)$, with $\beta = 1/k_BT$. The additive constant $cst(l)$ copes with the fact that the probabilities $p(R_{ee})$ are normalized with respect to the interval $[l;l+dl]$: the free energy is known up to an additive constant. If the same algorithm is applied for a set of overlapping intervals, the constant $cst(l)$ can be determined by continuity and the total free energy can be computed. In order to have a good sampling in each interval, its size dl has to be chosen carefully. If the energy in the interval $[l;l+dl]$ presents large variations, a limited sampling will explore only a small part of the interval. This is due to the Monte Carlo (MC) method of sampling that will spend most of the simulation with configurations having $\sim N_d k_B T$ of energy higher than the lowest energy, where N_d is the number of degrees of freedom of the system. Thus, the size of the interval needs to be chosen such as the maximum variation in energy of the interval is not superior to $N_d k_B T$.

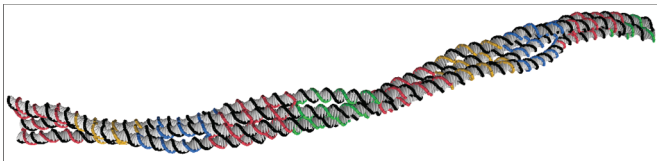

FIG. 5. (Color online) Structure of a 4-oDNA(298) after 10^6 MC steps (Sim 1).

III. TEST OF THE TWIST AND ELECTROSTATIC PARAMETERS

A. Twist parameter

In natural B-DNA, the twist between successive pairs of basis is slightly dependent on the sequence of bases [39]. The mean value obtained from crystallographic data of B-DNA structures is 35.45°. In the SOP model, the original parameters [30] give a mean value of the twist (Tw) 35.35°, very close to the experimental value. This value results from an equilibrium between the equilibrium length of the bond representing the phosphate backbone (6 Å) and the distance of minimal energy between ellipses which imposes a center to center distance of 3.3 Å. An accurate modeling of the natural twist is particularly important when dealing with oDNA. The design of these structures is based on the idea that origamis are stable if, locally, they preserve as much as possible the structure of the B-DNA double helix. This constrains the locations where

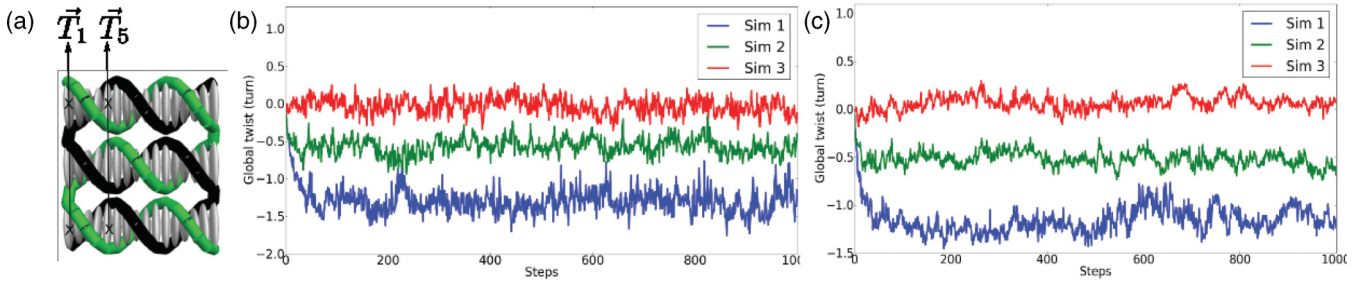

FIG. 6. (Color online) (a) Vectors $\mathbf{T}_1$ and $\mathbf{T}_5$ used to define the global twist of the structure, made here with $n = 3$ strands. (b) Evolution of the global twist Tw_g for a 2-oDNA (298) structure in the three simulations Sim 1, Sim 2, and Sim 3. (c) Same data for a 3-oDNA(298) structure. The sampling ratio is 210^7 MC steps.

crossovers can take place. Let us denote Tw_D as the value of the twist used to design the origami, and Tw_N as the natural twist adopted by weakly interacting helices in solution. In the Rothemund's seminal work [5], structures were designed with a twist $\mathrm{Tw}_D = 33.75^\circ$. This allows 1.5 turns for 16 base pairs, which simplifies the placement of the crossovers. But this also imposes a constraint to the real structure: origamis with $\mathrm{Tw}_D \neq \mathrm{Tw}_N$ are expected to be twisted in solution. In Ref. [40], the authors made TEM measurements on 3D compact oDNA structures, formed by stacked helices in a cubic lattice. The observed structures only led to a flat structure when assuming $\mathrm{Tw}_D = 34.48^\circ$ or $\mathrm{Tw}_D = 34.65^\circ$. Other combinations, including the one with $\mathrm{Tw}_D = \mathrm{Tw}_N$, led to twisted structures. This is surprising because nontwisted structures formed by helices packed in a honeycomb lattice have been observed with $\mathrm{Tw}_D = 10.5$ bp/turn [7]. This could be due to differences in the solvent characteristics (Mg concentration, ionic strength).

In order to illustrate these considerations, we realized three simulations on planar arrangements, noted n-oDNA(l), of $n = 2,3,4,\ldots$ helices with l base pairs each (cf. Figs. 4 and 5). These simulations are characterized by different values for the couples (Tw_N,Tw_D): Sim 1: $\mathrm{Tw}_N = 35.45^\circ$ and $\mathrm{Tw}_D = 33.7^\circ$; Sim 2: $\mathrm{Tw}_N = 34.48^\circ$ and $\mathrm{Tw}_D = 33.7^\circ$; Sim 3: $\mathrm{Tw}_N = 34.48^\circ$ and $\mathrm{Tw}_D = 34.48^\circ$.

$\mathrm{Tw}_N = 35.45^\circ$ is the value obtained with the parameters of Ref. [30]. $\mathrm{Tw}_N = 34.48^\circ$ can be obtained in the SOP model by changing the value of the bond's equilibrium distance from 6 Å(original value [30]) to 5.9 Å. The total length l of the n-oDNA(l) structures cannot be varied freely because the difference in orientations between the first and last base pairs needs to be close to 180°. Therefore, the total length minimizes $|l\mathrm{Tw}_D - 180^\circ|\mathrm{mod}(360^\circ)$. For Sim 1 and Sim 2, this yields $l = 315$ and for Sim 3, $l = 298$.

Given a value of Tw_D, the positions of crossovers are determined as follows. In n-oDNA(l) structures, a crossover takes place every three helical turns. If the first base pair is chosen as a reference, a base pair taking part in a crossover must have the same orientation as the first base pair in order to be able to connect to the neighbor helix. As a consequence, the first crossover corresponds to the i_1th base pair where i_1 minimizes $|\mathrm{Tw}_0 + i_1\mathrm{Tw}_D - 1080^\circ|$. In this expression, the twist of the first base pair Tw_0 is chosen equal to 10° for convenience. More generally, the index i_n of the base pair that forms the nth crossover minimizes $\delta T_c(n) = |\mathrm{Tw}_0 + i_n\mathrm{Tw}_D - n1080^\circ|$.

In Sim 1 and Sim 2, as $\mathrm{Tw}_D = 33.7^\circ$, the choice $i_n = 32n$ yields $\delta T_c(n) \ll 1^\circ$. In Sim 3, the distances between crossovers linking the first and second strand that minimize $\delta T_c(n)$ are 31, 31, 32, 31, 31, 32, 31, 31, 32. The location of the crossovers between the second and third strands were computed in a similar way.

Because we intend to compare our simulations to experimental data involving this type of compact structures, we will in the following adopt the value $\mathrm{Tw}_N = 34.48^\circ$. Let us now introduce a measure of the global twist. Let $\mathbf{T}_i$ be the vector that links the ith base pair in the first row to the ith base pair in the nth row (cf. Fig. 6 for an example representing $\mathbf{T}_1$ and $\mathbf{T}_5$ with $n = 3$) and let $\alpha(\mathbf{T}_i,\mathbf{T}_{i+1})$ be the angle formed by two successive $\mathbf{T}_i$ vectors. We define the global twist Tw_g of

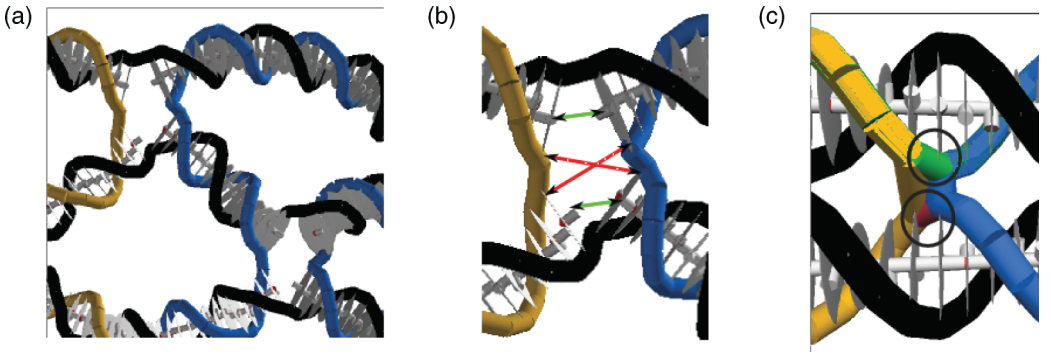

FIG. 7. (Color online) In the absence of additional bonds, the combined effect of electrostatic repulsion and stacking attraction leads to unstacking of base pairs (a). The zoom in (b) represents the electrostatic interactions as red (dashed) arrows, the stacking interactions as green (continuous) arrows. (c) Extra liaisons added at the crossover are in green and red and framed by two circles.

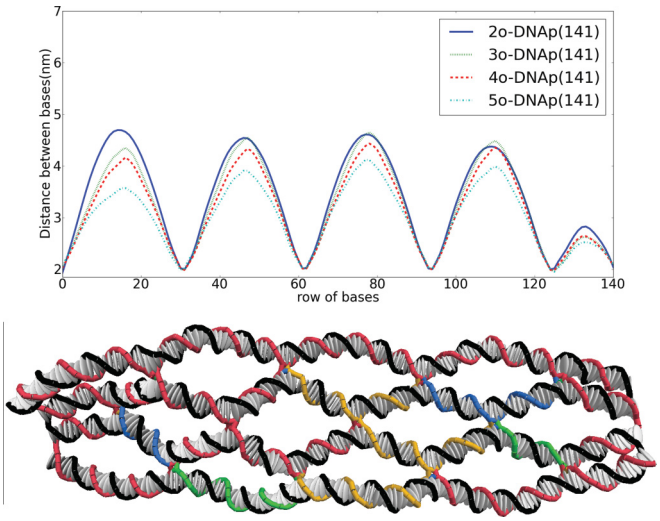

FIG. 8. (Color online) Distance between two neighbor strands as a function of the position along the strand. A typical origami structure is displayed below.

a n-oDNA(l) structure as the sum of the $\alpha(\mathbf{T}_i,\mathbf{T}_{i+1})$ angles along the strand:

$$\mathrm{Tw}_g = \sum_{i=1}^{l-1} \alpha(\mathbf{T}_i,\mathbf{T}_{i+1}). \tag{2}$$

Notice that this definition of the global twist is only meaningful if the twist fluctuations are more important in the direction along the helix axis than in the perpendicular direction. Figures 6(b) and 6(c) illustrate the results of the three simulations Sim 1, Sim 2, and Sim 3. In Sim 1, it is expected that $\mathrm{Tw}_g = 315(33.7 - 35.35)/360 = -1.37$ turns. In Sim 2, the expected value is -0.65 turns. Sim 3 has been designed in purpose to obtain $\mathrm{Tw}_g = 0$. The data in Fig. 6 confirm these expectations. In the following, we will continue to use $\mathrm{Tw}_D = \mathrm{Tw}_N = 34.48^\circ$ and denote the resulting planar structures as n-oDNA$_p$(l).

B. Electrostatic parameter

The distribution of charges along the DNA helix and the resulting effective charge parameters have been studied by many groups. In particular, several authors [35] suggest that an attenuated effective charge should be used in simulations of DNA. For DNA origamis, the situation is different. For instance, if one refers to the simulations in Ref. [34], it is clear that the presence of Mg can induce attraction between DNA helices provided those are free to reorient one with respect to the other. This is forbidden by the particular topology of DNA origamis. This is the main reason to keep the modeling of electrostatics as simple as possible: in the sequel, we only consider purely repulsive interactions Eq. (1), with no rescaling of the charges, the effect of the counterions being taken into account only through the existence of a finite Debye length that will be set to 10.5 Å.

With the introduction of the electrostatic interaction, a new problem appears. We find that in a typical MC trajectory, base pairs that participate in a crossover eventually become unstacked, as illustrated in Fig. 7(a). The stacking as defined in the original SOP model [30] is not attractive enough

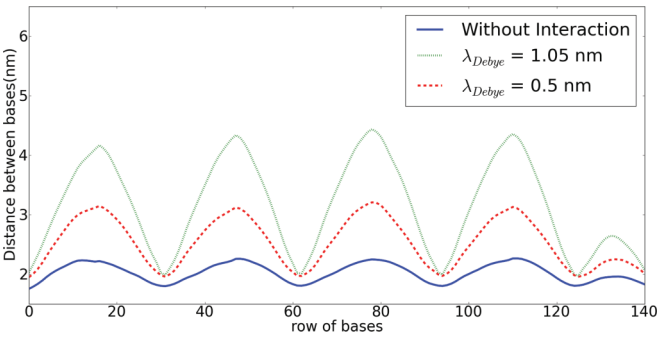

FIG. 9. (Color online) Distance between two neighbor strands as a function of the position along the strand. Comparison for three values of the Debye length.

to overcome the electrostatic repulsion. This situation is not found in more realistic, atom-based molecular dynamics simulations [41]. Calorimetry experiments [42] also suggest that such unstacking does not exist. To avoid the unstacking, we added two extra bonds between the base pairs that participate in a crossover, as illustrated in Fig. 7(c). These extra bonds have the same strength as those of the sugar-phosphate backbone.

The distance between two neighbor strands, as a function of the position along the strand, for several n-oDNA$_p$(l) structures, is given in Fig. 8. These values are obtained as averages over eight independent simulations, each with 2×10^{10} MC steps. The maximum of this distance is reached for the base pairs located halfway between the two crossovers in the middle of the structure. This maximum decreases as the number of strands increases, as the result of the combined repulsions between different strands. It is remarkable that the maximum distance found experimentally (3.9 nm) compares so accurately with the maximum distance found in the Monte Carlo simulations [4.1 nm for the 4-oDNA$_p$(141) and 3.9 nm for the 5-oDNA$_p$(141)]. The influence of electrostatics is clearly shown in Fig. 9, where the distance along the strands is compared for two values of the Debye length, and in the absence of electrostatics.

IV. PERSISTENCE LENGTH OF DNA ORIGAMIS

The previous section showed that the SOP model [30], with additional electrostatic interactions and a slight modification of

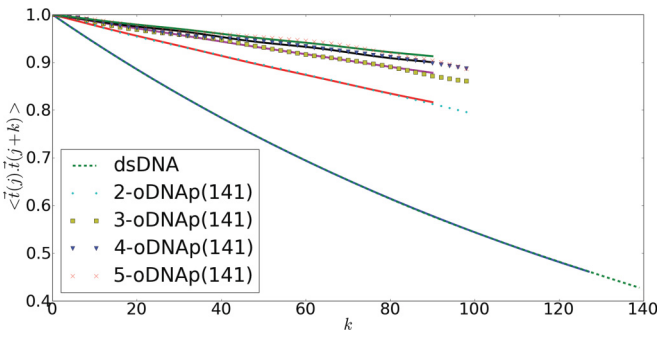

FIG. 10. (Color online) The correlation between the tangent vectors of a same strand as a function of the distance along the strand. For each structure, the symbols represent the measured correlation, the continuous lines represent the fitted data.

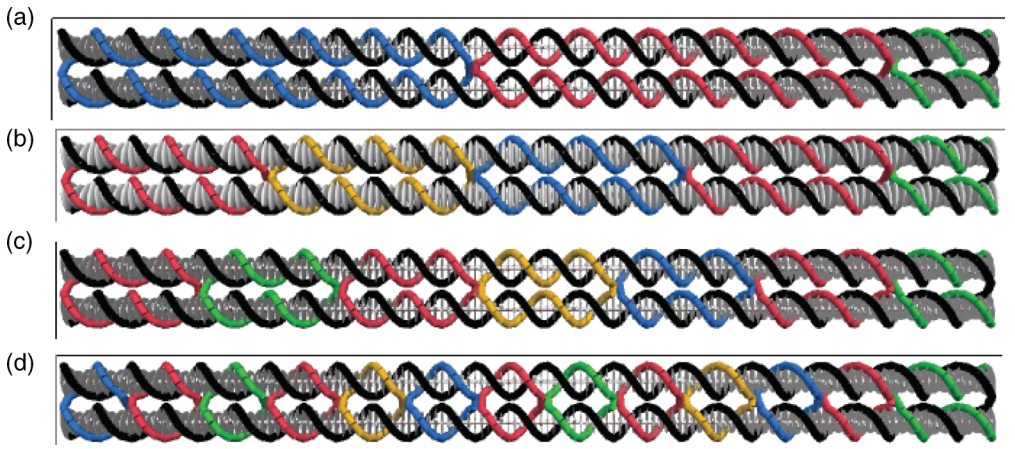

FIG. 11. (Color online) Four structures with 141 base pairs each and different distribution of the junctions, respectively (a) 4 crossovers, (b) 6, (c) 8, (d) 14. Notice that here we extend somewhat the notion of crossover to include the junctions at the ends.

the equilibrium length of the sugar-phosphate backbone, is able to reproduce static properties, such as the characteristic separation between strands as observed in AFM measurements, Fig. 1, and the absence of global twist for specific crossover distributions. In this section, we want to push the comparison further and compute the persistence length of DNA origamis.

A. Planar oDNA

For linear structures, the persistence length l_p is usually defined by the relation

$$\langle \mathbf{t}(j) \cdot \mathbf{t}(k) \rangle \sim e^{-|j-k|/l_p}, \tag{3}$$

where $\mathbf{t}(j)$ is the tangent vector at the position j along the thread. Implicitly, Eq. (3) assumes that the structure is homogeneous along the strand. This is not the case for oDNA, where the distances between crossovers constitute another characteristic length. In order to compute l_p, we coarse grain the oDNA structure with reference to the ideal situation where the base pairs B_{ij} are located on a regular grid where lines (index i corresponding to the dsDNA strands) and columns (index j, in the direction perpendicular to the lines) can be defined. The coarse graining is done in two steps. First, we average the position of the center of the ellipses belonging to a same column: $B_i^1 = \sum_j B_{i,j}$. In this way, a family of tangent vectors $\tau_i^1 = B_{i+1}^1 - B_i^1$ is obtained. Second, we average these tangent vectors along the i coordinate: $\tau_i^a = \sum_{l=i-\delta i}^{l=i+\delta i} \tau_l^1$. This averaged tangent vector field is used to compute the persistence length for structures containing more than one dsDNA strand.

Let us first consider the variation of l_p (Fig. 10) of several n-oDNA$_p$(141) structures as a function of the density of crossovers (cf. Fig. 11 and Table I). As expected, the structure with two parallel strands is generally stiffer than the double helix, with $l_p/l_p^0 \sim 3.2$ (here, $l_p^0 = 150$ bp denotes the persistence length of dsDNA). When only four crossovers are present [cf. Figs. 11(a) and 12(a)], we find that the persistence length of 2-oDNA$_p$(141) is lower than that of one single helix. This result can be understood by noticing that the crossovers are separated by 90 base pairs. Instead of being parallel, the dsDNA strands are almost free to fluctuate and the electrostatic repulsion between strands increases these fluctuations, leading to contorted structures with a persistence length inferior to that of a single dsDNA strand. It should also be noticed that these structures are difficult to describe by a single coordinate, the coarse-graining procedure reaching here its limit of validity.

Let us now consider the variation of l_p as a function of the number of rows, when the distance between crossovers is

TABLE I. Variation of the persistence length as a function of the number of crossovers for several types of 2-oDNA(141) structures. The 6c structure is identical to 2-oDNA$_p$(141).

No. crossovers	4c	6c	8c	14c
l_p/l_p^0	0.6 ± 0.3	3.2 ± 0.3	3.9 ± 0.3	3.9 ± 0.1
Tw$_g$ (turn)	0.0 ± 0.1	0.1 ± 0.1	0.1 ± 0.0	0.1 ± 0.0

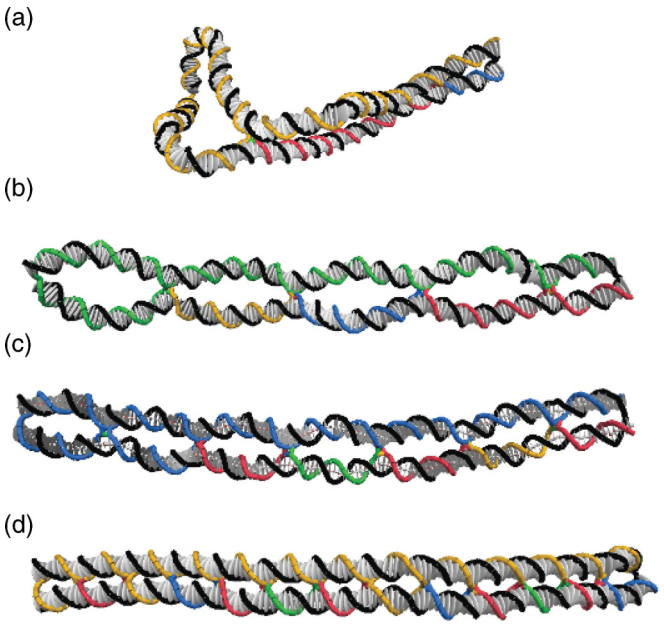

FIG. 12. (Color online) Four different structures with 141 base pairs each and different distribution of the junctions, respectively, (a) 4 crossovers, (b) 6, (c) 8, (d) 14. Typical configurations observed at the end of the MC simulations.

TABLE II. Variation of the persistence length as a function of the number of rows (helices). The length of each row is 298 base pairs, as in the original Rothemund rectangle.

	2-DNA$_p$(298)	3-DNA$_p$(298)	4-DNA$_p$(298)
l_p/l_p^0	3.5 ± 0.3	5.7 ± 0.7	7.4 ± 1.7
Tw$_g$ (turn)	0.1 ± 0.0	0.2 ± 0.1	0.1 ± 0.0

fixed to 31 (cf. Tables II and III, and see Fig. 13). For the structures with 298 base pairs per row (analog to the original Rothemund's rectangular origami), increasing the number of rows increases monotonously l_p, by roughly $1.8l_p^0$ added per row. For shorter structures (Table III), the situation is very similar, as should be expected for a local measure of elasticity.

To the best of our knowledge, there are no direct measurements of the elastic properties of planar origamis, but only indirect estimates of the persistence length. In Ref. [43], structures containing two antiparallel double helices, linked by two crossovers DAE structures separated by an even number of half turns were studied experimentally. A statistical analysis of the products of cyclization of DAE monomers led to the conclusion that the persistence length of these structures is around 2.7 times that of the double helix. We have simulated DAE structures of various lengths (cf. Fig. 14) and reached qualitatively similar results (Table IV): $l_p/l_p^0 \sim 3.3$.

B. Umbrella sampling of planar DNA origamis

Umbrella sampling simulations of planar n-oDNA$_p$(141) origamis were also performed in order to obtain an independent measurement of the persistence length of these structures. In these simulations, the end to end distance is constrained to be in overlapping intervals of length $\sim$1 nm. The variation of the averaged energy and force as a function of the end to end distance are represented in Fig. 15. These averaged quantities can be compared to the predictions of the WLC model. It has been shown [44] that for segment lengths longer than 10–15 nm the link between the persistence length l_p and the energy of bending of a dsDNA strand predicted by the WLC model is accurate:

$$E(\theta) = k_B T \frac{1}{2} \frac{l_p}{l} \theta^2. \tag{4}$$

Here, θ is the angle formed by two segments of length l. If R_{ee} denotes the end to end distance, $\cos(\theta/2) = R_{ee}/L_c$, where $L_c = 2l$ denotes the contour length. Therefore, the energy of a dsDNA with end to end distance R_{ee} is

$$E(R_{ee}) = k_B T \frac{1}{2} \frac{l_p}{L_c/2} \left[2 \arccos\left(\frac{R_{ee}}{L_c} \right) \right]^2, \tag{5}$$

TABLE III. Variation of the persistence length as a function of the number of rows (helices). The length of each row is 141 base pairs.

	2-DNA$_p$ (141)	3-DNA$_p$ (141)	4-DNA$_p$ (141)	5-DNA$_p$ (141)
l_p/l_p^0	3.2 ± 0.3	5.1 ± 0.4	5.8 ± 1.4	6.6 ± 3.3
Tw$_g$ (turn)	0.1 ± 0.0	0.1 ± 0.1	0.2 ± 0.0	0.2 ± 0.0

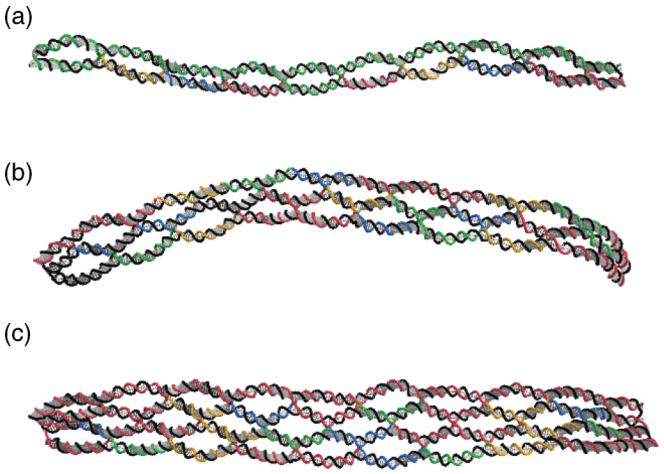

FIG. 13. (Color online) Typical configurations obtained after MC equilibration for three different structures with 298 base pairs each, with, respectively (a) 2 rows, (b) 3 rows, and (c) 4 rows.

and the corresponding force is

$$F(R_{ee}) = 8k_B T \frac{l_p}{L_c^2} \frac{\arccos(R_{ee}/L_c)}{\sqrt{1-(x/L_c)^2}}. \tag{6}$$

This force is almost constant $\sim 8k_B T l_p/L_C^2$ for the range of R_{ee} values considered here. The data in Fig. 15 yield $l_p = 2.4l_p^0$ for 2-DNA$_p$(141) and $l_p = 5.8l_p^0$ for 5-DNA$_p$(141), compatible with the values obtained in the Monte Carlo simulations without constraints (Table III).

C. Persistence length of a 3D DNA origami

The work of Kauert *et al.* [28] reports direct magnetic tweezers measurements made on 3D o-DNA. These are bundles of four or six DNA helices with enlarged ends that allow tight binding to either a surface or a magnetic bead. Values for the bending and torsional rigidities were obtained by optically monitoring the position of the bead. The bead fluctuations were compared to Monte Carlo simulations of the wormlike chain model. Very good agreement was

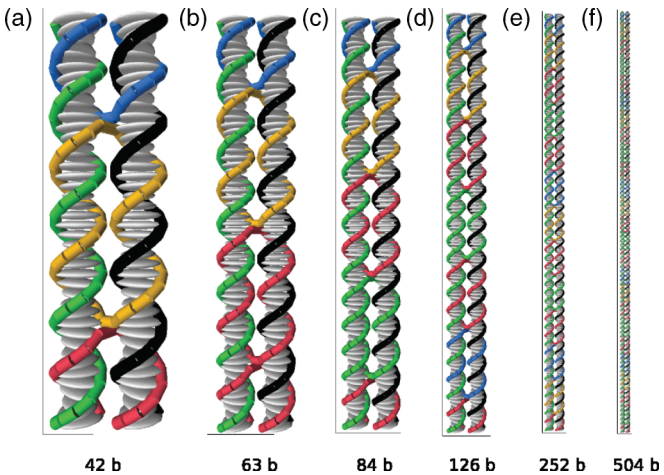

FIG. 14. (Color online) Structure of the simulated DAE structures. For each structure, the total number of bases is indicated at the bottom.

TABLE IV. Normalized persistence length as a function of the number of DAE monomers. The corresponding structures are illustrated in Fig. 14.

	DAE	2-mer	3-mer	5-mer	11-mer	21-mer
l_p/l_p^0	3.1 ± 0.1	3.4 ± 0.2	3.6 ± 0.2	3.7 ± 0.2	3.8 ± 0.1	3.5 ± 0.2

obtained between the simulated and observed fluctuations, with corresponding bending rigidities 16 (four helix bundle) and 40 (six helix bundle) times that of the dsDNA.

We modelled structures similar to the four helix bundle (Fig. 16). A shattered version of the structure is also presented in Fig. 16. Our design links together two 2-oDNA$_p$ structures. The junctions between the two 2-oDNA$_p$ are located at the base pairs where the crossover distances are minimum (red circles in Fig. 16). The persistence length of two such structures are reported in Table V. Again, we find good agreement between the Monte Carlo simulations and the experimental results obtained with magnetic tweezers.

TABLE V. Normalized persistence length for the four helix bundles (Fig. 16) as a function of the number of monomers.

4-helix bundle	2-mer	4-mer
l_p/l_p^0	16.6 ± 2.5	17.5 ± 6.3

V. DISCUSSION

In this paper, we have used Monte Carlo sampling to describe in a coarse-grained way the fluctuations of nanostructures made of DNA. We have modified the original force field [30] in two ways. First, the equilibrium length of the sugar-phosphate bonds has been slightly reduced. Second, we added screened electrostatic interactions between sites in different strands to account for the characteristic bending of double helices in planar origamis [5], as observed by AFM.

We have first considered planar structures. As long as the transverse dimension (given by the number of helices) is small compared to the length of the helices, the structures can still be characterized as linear structures with a persistence length. For bundles of two helices, $l_p/l_p^0 \sim 3$, in qualitative agreement with experimental data from the Seeman's laboratory [43]. When increasing the number of helices N_h, our data are consistent with $l_p/l_p^0 \sim 1.7N_h$. The situation can be compared to that of a polymer trapped in two dimensions. In this case, the persistence length increases by 2 [45]. In oDNA structures the helices are similarly trapped because the fluctuations in the width of the structures are limited by steric hindrance and electrostatic repulsion.

All these data can be consistently obtained both from equilibrium Monte Carlo simulations and umbrella sampling simulations. Finally, we have also modelized four-helix bundles similar to the structures considered in Ref. [28]. The bending rigidity of this structure is ~17 times that of a dsDNA, in good agreement with the experimental data obtained with magnetic tweezers in Ref. [28].

An important point in the modeling of DNA origamis is the treatment of the crossover regions. The point of view adopted in this work is that the stacking between bases is preserved in the crossover. We have mentioned both experimental [42] and numerical [41] data that support this point of view. One could also argue that base unpairing at crossovers would be incompatible with the observed sensitivity of the global twist versus the twist of design. However, other high temperature simulations [46] suggest that base unstacking at crossovers is possible. Further experimental characterization of crossover regions is clearly needed.

The approach advocated here seeks to obtain a convenient coarse-grained modeling of DNA origami structures starting from an existing model for single dsDNA molecules. As explained in the Introduction, mostly continuum mechanics approaches [29] have been used in the past to address this problem. Two basic differences with the finite-element methods should be pointed out. First, the absence of electrostatics

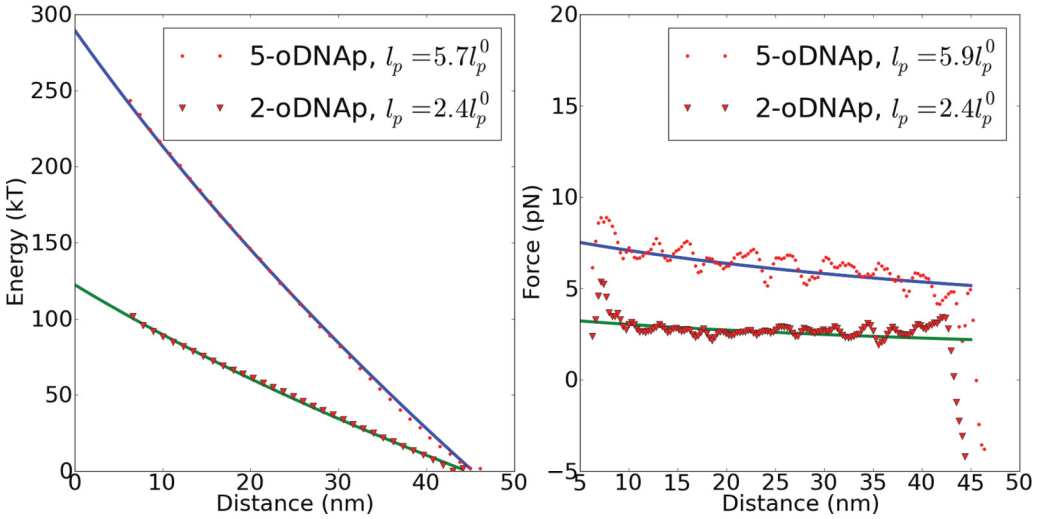

FIG. 15. (Color online) Umbrella sampling simulations of 2-DNA$_p$(141) and 5-DNA$_p$(141) structures. The end-to-end distance is varied from 7 to 45 nm, with overlapping intervals of length 1 nm. The data from the umbrella sampling are fitted by an analytic WLC model (continuous lines). Left panel: energy. Right panel: force.

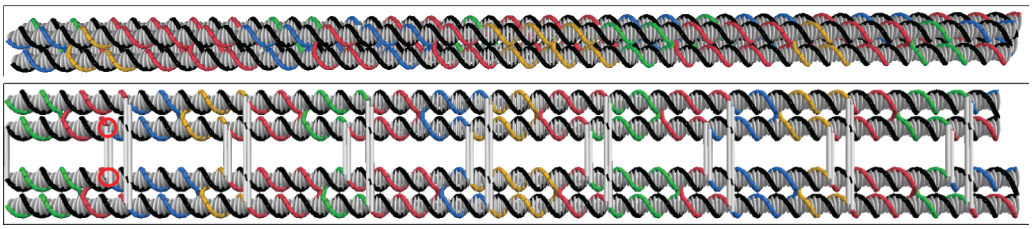

FIG. 16. (Color online) Structure of an oDNA similar to the four-helix bundle of Ref. [28]. Top: side view of the structure. Bottom: shattered view of the same structure. The circles in the bottom panel show how the links between the two 2-oDNA$_p$ structures are determined.

leads to equilibrium structures that deviate from the AFM observations shown in Fig. 1. In our opinion, this could be a particularly limiting factor to describe structures that are loosely tightened (when the distance between crossovers increases). Second, the finite-element method relies on the equipartition theorem to describe thermal fluctuations, and the use of normal modes to describe these fluctuations. In this respect, Monte Carlo simulations have a broader range of applicability. On the other hand, finite-element computations are much faster than the MC simulations presented here. In this sense, a combined use of both methods could constitute a powerful approach to the modeling of DNA nanostructures. Further extensions or improvements of the model should also include the possibility of base-pair opening. As pointed out recently [47], short double DNA strands show extreme bendability. This could be explained by the existence of frequent kink or bubble formations, even though anharmonic elasticity cannot be ruled out.

[1] H. Yan, S. H. Park, G. Finkelstein, J. H. Reif, and T. H. LaBean, Science **301**, 1882 (2003).
[2] N. C. Seeman, Nature (London) **421**, 427 (2003).
[3] R. P. Goodman, I. A. T. Schaap, C. F. Tardin, C. M. Erben, R. M. Berry, C. F. Schmidt, and A. J. Turberfield, Science **310**, 1661 (2005).
[4] J. Malo, J. C. Mitchell, C. Vńien-Bryan, J. R. Harris, H. Wille, D. J. Sherratt, and A. J. Turberfield, Angew. Chem. Int. Ed. **44**, 3057 (2005).
[5] P. W. K. Rothemund, Nature (London) **440**, 297 (2006).
[6] E. S. Andersen, M. Dong, M. M. Nielsen, K. Jahn, R. Subramani, W. Mamdouh, M. M. Golas, B. Sander, H. Stark, C. L. P. Oliveira, J. S. Pedersen, V. Birkedal, F. Besenbacher, K. V. Gothelf, and J. Kjems, Nature (London) **459**, 73 (2009).
[7] S. M. Douglas, H. Dietz, T. Liedl, B. Högberg, F. Graf, and W. M. Shi, Nature (London) **459**, 414 (2009).
[8] H. Dietz, S. Douglas, and W. M. Shih, Science **325**, 725 (2009).
[9] S. B. Smith, L. Finzi, and C. Bustamante, Science **258**, 1122 (1992).
[10] S. B. Smith, Y. Cui, and C. Bustamante, Science **271**, 795 (1996).
[11] P. Cluzel, A. Lebrun, C. Heller, R. Lavery, J.-L. Viovy, D. Chatenay, and F. Caron, Science **271**, 792 (1996).
[12] B. Essevaz-Roulet, U. Bockelmann, and F. Heslot, Proc. Natl. Acad. Sci. USA **94**, 11935 (1997).
[13] J. Allemand, D. Bensimon, R. Lavery, and V. Croquette, Proc. Natl. Acad. Sci. USA **95**, 14152 (1998).
[14] C. R. Calladine and H. R. Drew, J. Mol. Biol. **178**, 773 (1984).
[15] R. E. Dickerson, Nucl. Ac. Res. **17**, 1797 (1989).
[16] X. J. Lu and W. K. Olson, J. Mol. Biol. **285**, 1563 (1999).
[17] W. K. Olson *et al.*, J. Mol. Biol. **313**, 229 (2001).
[18] T. E. Ouldridge, A. A. Louis, and J. P. K. Doye, Phys. Rev. Lett. **104**, 178101 (2010).
[19] J. F. Marko and E. D. Siggia, Macromolecules **27**, 981 (1994).
[20] J. F. Marko and E. D. Siggia, Macromolecules **28**, 8759 (1995).
[21] T. T. Perkins, D. E. Smith, R. G. Larson, and S. Chu, Science **268**, 83 (1995).
[22] T. Schlick and W. K. Olson, J. Mol. Biol. **223**, 1089 (1992).
[23] G. Chirico and J. Langowski, Biopolymers **34**, 415 (1994).
[24] H. Schiessel, J. Widom, R. F. Bruinsma, and W. M. Gelbart, Phys. Rev. Lett. **86**, 4414 (2001).
[25] P. W. K. Rothemund, A. Ekani-Nkodo, N. Papadakis, A. Kumar, D. K. Fygenson, and E. Winfree, J. Am. Chem. Soc. **126**, 16344 (2004).
[26] T. Liedl, B. Högberg, J. Tytell, D. E. Ingber, and W. M. Shih, Nat. Nanotechnol. **5**, 520 (2010).
[27] P. OâNeill, P. W. K. Rothemund, A. Kumar, and D. K. Fygenson, Nano Lett. **6**, 1379 (2006).
[28] D. J. Kauert, T. Kurth, T. Liedl, and S. Siedel, Nano Lett. **11**, 5558 (2011).
[29] D. Kim, F. Kilchherr, H. Dietz, and M. Bathe, Nucleic Acids Res. **40**, 2862 (2012).
[30] B. Mergell, M. R. Ejtehadi, and R. Everaers, Phys. Rev. E **68**, 021911 (2003).
[31] T.-J. Fu and N. C. Seeman, Biochemistry **32**, 3211 (1993).
[32] N. Bruant, D. Flatters, R. Lavery, and D. Genest, Biophys. J. **77**, 2366 (1999).
[33] A. Kornyshev, D. Lee, S. Leikin, and A. Wynveen, Rev. Mod. Phys. **79**, 943 (2007).
[34] B. Luan and A. Aksimentiev, J. Am. Chem. Soc. **130**, 15754 (2008).
[35] X. Qiu, K. Andresen, L. W. Kwok, J. S. Lamb, H. Y. Park, and L. Pollack, Phys. Rev. Lett. **99**, 038104 (2007).
[36] D. Frenkel and B. Smit, *Understanding Molecular Simulation: From Algorithms to Applications* (Academic, London, 2002).
[37] D. Chandler, *Introduction to Modern Statistical Mechanics* (Oxford University Press, New York, 1987).
[38] P. Virnau and M. Müller, J. Chem. Phys. **120**, 10925 (2004).

[39] A. Gorin, V. Zhurkin, and K. Wilma, J. Mol. Biol. **247**, 34 (1995).
[40] Y. Ke, S. Douglas, M. Liu, J. Sharma, A. Cheng, A. Leung, Y. Liu, W. Shih, and H. Yan, J. Am. Chem. Soc. **131**, 15903 (2009).
[41] P. Maiti, T. Pascal, N. Vaidehi, J. Heo, and W. Goddard, Biophys. J. **90**, 1463 (2006).
[42] L. A. Marky, N. R. Kallenbach, K. A. McDonough, N. Seeman, and K. J. Breslauer, Biopolymers **26**, 1621 (1987).
[43] P. Sa-Ardyen, A. V. Vologodskii, and N. C. Seeman, Biophys. J. **84**, 3829 (2003).
[44] P. Wiggins *et al.*, Nat. Nanotech. **1**, 137 (2006).
[45] L. D. Landau and E. M. Lifshitz, *Statistical Physics*, Part 1, 3rd ed. (Pergamon, Oxford, NY, 1980).
[46] J. Yu, T. Ha, and K. Schulten, Nucleic Acids Res. **32**, 6683 (2004).
[47] R. Vafabakhsh and T. Ha, Science **337**, 1097 (2012).